Visualization Of Aerial Color Imagery Through Shadow Effect Correction

Hong-Gyoo Sohn
Kong Hyun Yun
Dept. of Civil and Environment Engineering, Yonsei University, South Korea
sohn1@yonsei.ac.kr
ykh1207@yonsei.ac.kr

In-Tae Yang
Dept. of Civil Engineering, Kangwon National University, Korea
intae@kangwon.ac.kr

Kangwon Lee
Hanjin Information Systems & Telecommunication Co., Ltd., Korea
kwlee@hist.co.kr

Abstract

Correction of shadow effects is critical step for image interpretation and feature extraction from aerial imagery. In this paper, an efficient algorithm to correct shadow effects from aerial color imagery is presented. The following steps have been performed to remove the shadow effect. First, the shadow regions are precisely located using the solar position and the height of ground objects derived from LIDAR (Light Detection and Ranging) data. Subsequently, segmentation of context regions is implemented for accurate correction with existing digital map. Next step, to calculate correction factor the comparison between the context region and the same non-shadowed context region is made. Finally, corrected image is generated by correcting the shadow effect. The result presented here helps to accurately extract and interpret geo-spatial information from aerial color imagery

Introduction

Recently, with the appearance of high spatial satellite and aerial color mage it is possible to recognize or extract urban geo-spatial information more precisely. However, due to complexity of diverse features in urban areas, accurate feature recognition is laborious task in imagery. Especially hidden area occurrence caused by buildings and radiometric distortion by shadow effects make processing more difficult. Hidden areas can be compensated by using multi-view images (Rau et al., 2002). Owing to the characteristic of cast shadow occurrence regardless of sensor position, however, correction for shadowed area is not easy. To deal with shadow effects in remote sensing images, attempts at correcting gray values which are dimmed by cast shadows have been made (Crippen et al., 1998; Civco, 1989; Pouch and Compagna, 1990; Colby, 1991; Richter, 1998; Rau et al. 2002). Most of researches are mainly focused on mountainous terrain in satellite imagery. Rau and others (2002) observed that shadow effects can be corrected by histogram matching method which are applied for between a shadow area and its surroundings.

For the correction of shadow effects, it is first necessary to delineate shadow regions. Shadow regions can be extracted by using solar position and DSM(Digital Surface Model). In other words, cast shadows, for the every pixel of the image, can be determined by tracing a straight line to the solar position over DSM at the time of image acquisition (Giles, 2001). Richter (1998) developed algorithms to efficiently determine the horizon for all pixels of study area in grid DEM (Digital Elevation Model) and it could be adapted to determine the shadow regions (Brown, 1991). Also, Giles (2001) first evaluated quantitatively the results of a cast-shadow delineation program with a spatial comparison of areas marked by a human interpreting cast shadows in a Landsat TM image.

The proportion of shadow regions in aerial image mainly depends on the two factors: first, the height of buildings on the terrain and second, the solar elevation angle. Higher buildings and lower solar elevation angle both result in larger shadow regions. In this article, precisely to locate cast shadow regions in urban area, LIDAR data was selected for the generation of DSM, because it was reported that the elevation accuracy of LIDAR data is approximately ± 15 cm (Cowen et al.,2000). Also, for the accurate correction of shadow effects segmentation of shadow regions are necessary because delineating shadows fall on various types of backgrounds. The backgrounds included soil, grass, concrete, asphalt and so forth. However, shadow regions are mainly composed of low gray value so that segmentation task is very difficult. In this research, segmentation was implemented by using existing digital map containing surface cover types.

Details Of Study Area And Data Used

The data set for this study is composed of LIDAR data, digital map of 1:1000 scale and color aerial image containing some part of Sungnam city, Korea. The image was acquired on 10 November 2002, with solar elevation of 29.793° and solar azimuth 179.389°. Solar positions are calculated by the acquisition time and latitude of study area. Detail calculation is described later section. The ground resolution of the image is 25cm. Also the image was orthogonalized and georeferenced to DEM by ERDAS IMAGINE software. The DEM was created by TIN (triangulated irregular network) method using spot heights and elevation contour of digital map, and are converted into grid format at 25cm spacing. A 412 × 400 pixel of study area contains various patterns of urban facilities. The shadows of image mainly cast on buildings, trees, streets, roads and so forth. The height of ground is approximately from 30 to 55 meters from mean sea level. For shadow effect correction each blue, green and red images were produced from color image. After final process in this study color image was generated through combination of RGB images. The building height came from LIDAR which is an active technique to acquire 3-D information describing the land surface. It was reported that a typical system can provide data with 50cm horizontal accuracy and 15cm vertical accuracy. The LIDAR data was registered into images and digital map by human manipulation.

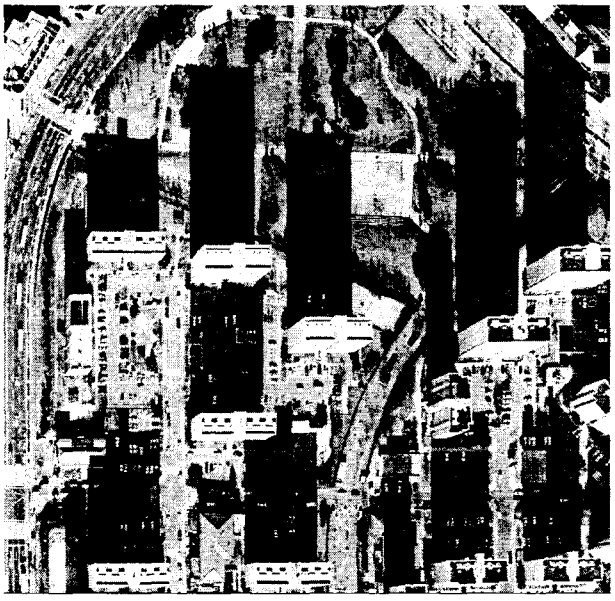

Fig. 1. Aerial color image of study area

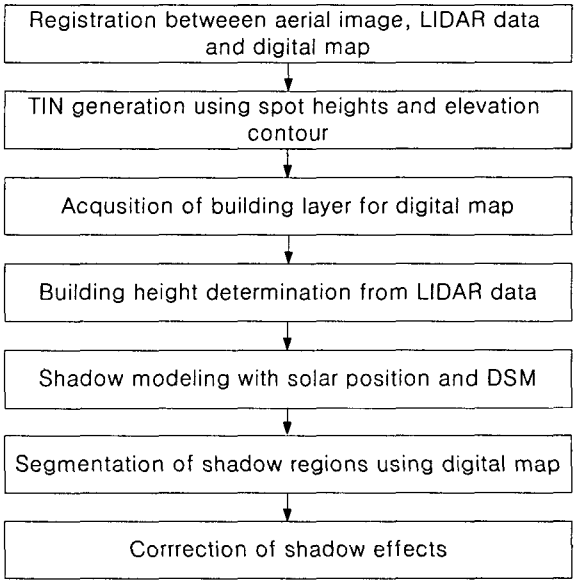

Fig. 2. schematic diagram of the proposed method

The Proposed Scheme

Figure 2 shows the schematic diagram of the propose method. First, registration should be processed between aerial color image, LIDAR data, and digital map. LIDAR data (WGS84 coordinate) must be transformed into TM coordinate being used in national coordinate system in Korea, because three data sets must have same coordinate system. Also, due to horizontal error of LIDAR data, it should be registered into aerial image or digital map precisely. In this research, peak points of LIDAR data between building boundary and ground are used for registration. Difference of coordinate between peak points and building boundary of image are calculated and used for horizontal shift of all LIDAR data. Secondly, a grid DEM was produced by using elevation contour and spot heights from digital map of 1:1000. Next, building layer extraction is required from digital map. A digital map contains many urban related features. Among them, building polygon was extracted from digital map. The building is represented as a single polygon in digital map. However, as shown in figure 1, the upper part of building was not flat but undulating. For the accurate shadow modeling, a polygon representing rising part of building is added in building layer. Therefore, building heights which are acquired as mean value of LIDAR data within each polygon are entered. Subsequently, shadow regions are delineated through shadow modeling by using solar position and produced DSM (digital surface model). Next stage, shadow regions are segmented for the accurate shadow effect correction with the help of digital map. Finally, shadow effects are corrected for the segmented shadow region.

Modeling Of Shadow Regions

The purpose of modeling of shadow regions is to calculate shadow length by using height data from LIDAR data and sun elevation angle and azimuth of aerial image.

Determination of building height from LIDAR data

Before modeling of shadow regions, accurate height value of building must be acquired for the precise shadow effect correction. The building height can be acquired directly by using LIDAR data. The LIDAR data within building polygon has two homogeneous values. The one represents the height of the bulk part of building, the other means building height except bulk part. However, the building polygon is represented as one polygon in digital map. To solve this problem, a polygon representing bulk part of building is added. Delineation of boundary between bulk part and other part was processed. In other words, one polygon was created by grouping peak points which are above 1.0 m in comparison with average of LIDAR data within polygon. Figure 3 shows the modified building polygon of study area. Figure 4 represents the LIDAR data within polygon.

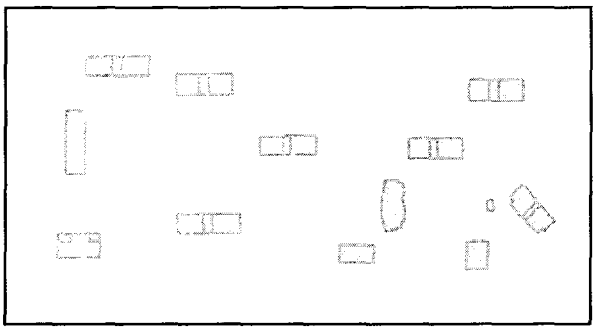

Fig. 3. modified building polygon of study area

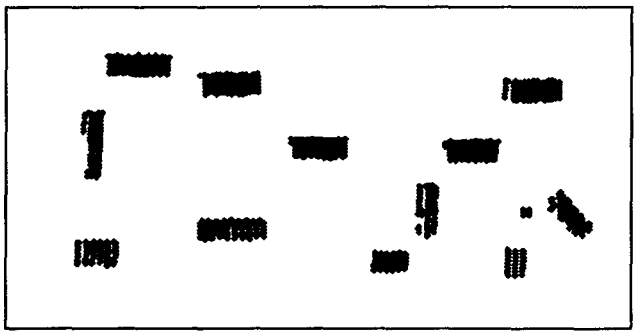

Fig. 4. LIDAR data within building polygon

Calculation of solar position

For the modeling of shadow regions, in addition to building height, solar positions are required at the time of image acquisition. To calculate solar position (sun elevation angle, azimuth), accurate time, date, latitude and longitude of study area are needed. The image was acquired on 10 November 2002 at 11:19 am. The longitude of study area is 127° 6′ 58″ and latitude is 37° 22′ 01″. If we can acquire the building height and sun elevation angle the modeling of shadows is possible. Figure 5 represents the geometry between building height, elevation angel and length of shadow in 1 dimension.

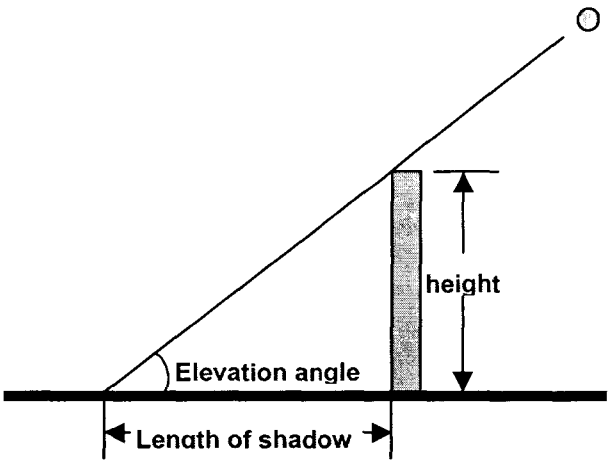

Fig. 5. The geometry between height, elevation angel and length of shadow at fixed azimuth

The calculation of solar elevation angel and azimuth done as follows.

First, the fractional year (γ) is calculated, in radians.

$$\gamma = \frac{2\pi}{365}(day\_of\_year - 1 + \frac{hour - 12}{24}) \quad (1)$$

From γ, we can estimate the equation of time(in minutes) and the solar declination angle (in radians).

$$eqtime = 229.18\times(0.000075 + 0.001868\cos\gamma - 0.032077\sin\gamma - 0.014615\cos 2 - 0.040849\sin 2\gamma) \quad (2)$$

$$decl = 0.006918 - 0.399912\cos\gamma + 0.070257\sin\gamma - 0.006758\cos 2\gamma + 0.000907\sin 2\gamma - 0.002697\cos 3\gamma + 0.00148\sin 3\gamma \quad (3)$$

Next, the true solar time is calculated in the following two equations. First the time offset is found, in minutes, and then the true solar time, in minutes.

$$time\_offset = eqtime - 4\times longitude + 60\times time\_zone \quad (4)$$

where eqtime is in minutes, longitude is in degrees, time zone is in hours from UTC (Mountain Standard Time = +7 hours).

$$tst = hr\times 60 + mn + sc/60 + time\_offset \quad (5)$$

where hr is the hour, mn is the minute, sc is the second.

The solar hour angle *(ha)*, in degrees, is:

$$ha = (tst/4) - 180 \quad (6)$$

The solar zenith angle (ω) can then be found from the following equation:
where *lat* means latitude.

$$\cos(\omega) = \sin(lat)\sin(decl) + \cos(lat)\cos(decl)\cos(ha) \quad (7)$$

Also, solar elevation angle(h) can be calculated by equation, $h = 90° - \omega$
And the solar azimuth (θ, clockwise from north) is:

$$\cos(180 - \theta) = -\frac{\sin(lat)\cos\omega - \sin(decl)}{\cos(lat)\sin\omega} \quad (8)$$

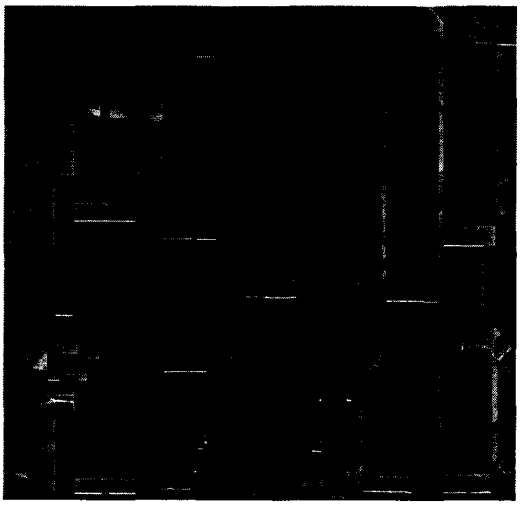

Fig. 6. Result of shadow modeling

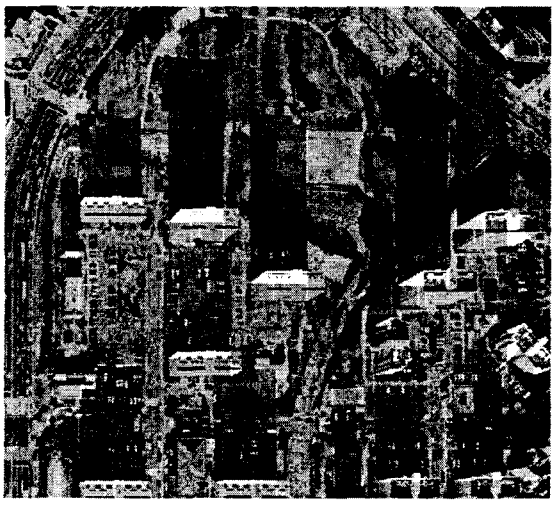

Fig. 7. Comparison modelling image with original image

Assessment of shadow modeling result

To evaluate the accuracy of the shadow modeling algorithm, cast shadows in the corresponding aerial color image compared to the output. For this purpose, a volunteer was recruited to independently interpret shadow regions in the aerial image based on the patterns of reduced gray values. This practitioner was experienced in

interpreting aerial images and, apart from being given instructions to this work. The human interpretation of shadow regions was assumed to be precisely correct. Figure 7 shows the comparison between the pixels representing red color marked by proposed algorithm and original image. Comparing the regions marked by the human volunteer to those delineated by proposed shadow modeling shows that overall accuracy was 97.62 percent. Table 1 illustrates the result of shadow modeling. The number in table 1 represents the pixel which are extracted, and reference data means human interpretation results

The errors(wrong detected or not detected) happened by using proposed algorithms are mainly caused by error of building height from LIDAR data. That error is described by following equation. The following equation is represented by geometry in figure 5.

$$s = \frac{h}{\tan \alpha} \tag{9}$$

where, h means building height, α is solar elevation angle and s represents the length of shadow.

As mentioned earlier, the vertical error of LIDAR data is ±15 cm and solar elevation angle is 29.793°. Therefore, the influence caused by elevation error is approximately 0.28 m. Because the ground resolution is 0.25 m/pixel, the wrong or undetected pixel of shadow region is ± 1~2 pixel. Besides, it is assumed that mapping error of building from digital map, DEM error, geometric correction error of aerial image can influence on shadowing modeling

Table 1. Error matrix resulting from shadow modeling

Category		*Reference data*		
		Shadow	*Non-Shadow*	*Total*
Modelling data	*Shadow*	*571963*	*15144*	*587107*
	Non-Shadow	*13925*	·	*13925*
	total	*585888*	*15144*	·

Segmentation Of Shadow Regions

Segmentation task of shadows is very important, because the results of segmentation have an effect on the correction of shadow effects directly. Shadow regions contain many different surface cover types and each cover type has a different spectral reflectance. According to each surface type, the degree of the influence interfered by shadow is also different. Therefore, the segmentation task is necessary. Polidorio (2003) suggested a technique to segment shaded areas in aerial color images. This method is based on the physical phenomenon of atmospheric dispersion of sun light, most well known as the Rayleigh scattering effect and very effective. Because the result showed that shadow regions are not clearly segmented, this method was not relevant. In this study, a digital map was utilized for segmentation.

Through overlapping extracted shadow region and polygons representing each surface type from digital map, the segmentation task was implemented. Figure 8 and Figure 9 illustrate the process of the proposed segmentation scheme. In figure 8, red color polygon was the result of shadow modeling, and cyan color polygons represent each surface cover type.

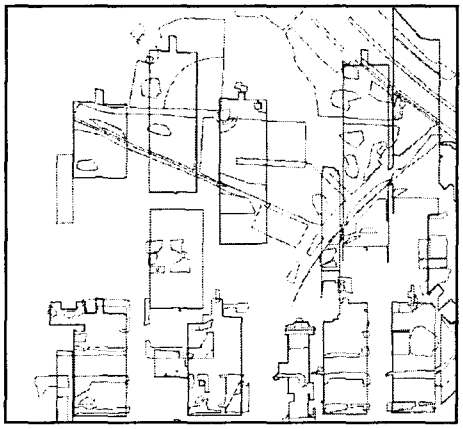

Fig. 8. display of two data sets overlaid

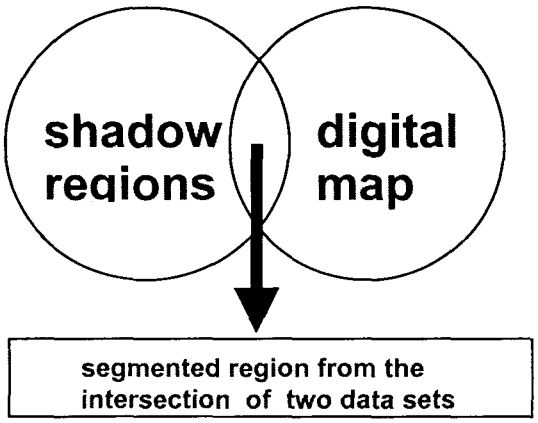

Fig. 9. extraction of intersection area

Algorothms For Shadow Effect Correction

Stockham (1972) recognized that an image is consisted of two components. 1) The amount of source light incident on the scene being viewed and 2) The amount of image point to reflect light. They are called the illumination and reflectance components. The image can be modelled as a product of two components, $I_{i,j} = r_{i,j} \times L_{i,j}$ The parameter, $L_{i,j}$, represents the illumination source and $\alpha_{i,j}$ is the reflectivity function of the image. The model of the image hindered by a shadow can be expressed as $I'_{i,j} = \alpha_{i,j} \times r_{i,j} \times L_{i,j}$. To generate shadow-free image the attenuation factor of the shadow, $r_{i,j}$, must be calculated and removed.

For the purpose of this study, the equation, $I'_{i,j} = \alpha_{i,j} r_{i,j} L_{i,j}$, can be modified as follows.

$$\frac{I'}{\alpha_{i,j}} = r_{i,j} L_{i,j} \tag{10}$$

$$\frac{I'}{\alpha_{i,j}} = I' - I'(1 - \frac{1}{\alpha_{i,j}}) \tag{11}$$

$$I' - I'(1 - \frac{1}{\alpha_{i,j}}) = r_{i,j} L_{i,j} \tag{12}$$

$$I' - k = r_{i,j} L_{i,j} \tag{13}$$

$$I' - k = I \tag{14}$$

Modified equation (14) means that the original pixel not hindered by shadow can be created by correcting the factor, k, to the pixel interfered by shadow. In this study, the correction factor is defined as k. Finally, if the correction factors for each segmented shadow region are calculated the correction of shadow effect is possible. The correction factor can be calculated by obtaining the difference between the average of shadow region and average of the same surface type region which is shadow-free.

Before applying equation (14) to the correction of shadow effect, three basic assumptions to accomplish shadow treatment in aerial image are considered. Three assumptions are following.

- *Complete information loss of region hindered by shadow does not occur.*
- *The influence of cast shadow occurred by each object is uniform.*
- *The DN value of similar surface cover characteristic is uniform.*

The first assumption considers that the DN values of shadowed area must not be zero. If the DN values are zero, the recovery of original information is impossible. In reality, the range of image values of shadow regions is not zero but very low in satellite and aerial images. The second assumption means that the influence of cast shadow caused by blocking of building must be uniform. Strictly speaking, the influence of shadows near building is more intensive than that of shadows which are located relatively further from building. However, the difference is very small. Based on this assumption, only one correction factor can be applicable to radiometric correction for segmented shadow areas. The third assumption explains that the standard deviation of DN values representing one segmented shadow region must be almost zero. If so, the accurate correction of shadow effect is possible. In reality, one segmented feature of shadow regions in aerial image shows the slight difference of DN values.

Following equation (15) and (16) was applied for this study.

$$O^t_{R,G,B}(x,y) = I^t_{R,G,B}(x,y) + k \tag{15}$$

$$k = I^r_{R,G,B}(m) - I^t_{R,G,B}(m) \tag{16}$$

where, $O^t_{R,G,B}(x,y)$: DN value of output image at each band.

$I^t_{R,G,B}(x,y)$: DN value of original image at each band.

$I^r_{R,G,B}(m)$: mean value of reference area at each band.

$I^t_{R,G,B}(m)$: mean value of target area at each band.

In equation (16), target area means the shadowed region to correct, and reference area represents the corresponding non-shadowed region.

Results and evaluation of shadow effect correction

In figure 10, the corrected image was created by the proposed algorithm. In comparison with original image the result shows more enhanced interpretability of aerial color image. The radiometric correction of asphalt road was very successful. The regions containing diverse and complex ground features show relatively low correction effect. For example, parking lot that is paved asphalt includes randomly distributed cars, but it is not unique single polygon that was included in digital map. Wrong correction of shadow effect occurred accordingly. From the viewpoint of interpretation of urban facilities its influence can be ignored. Table 2 illustrates average and standard deviation of main surface cover types, before and after applying shadow effect correction.

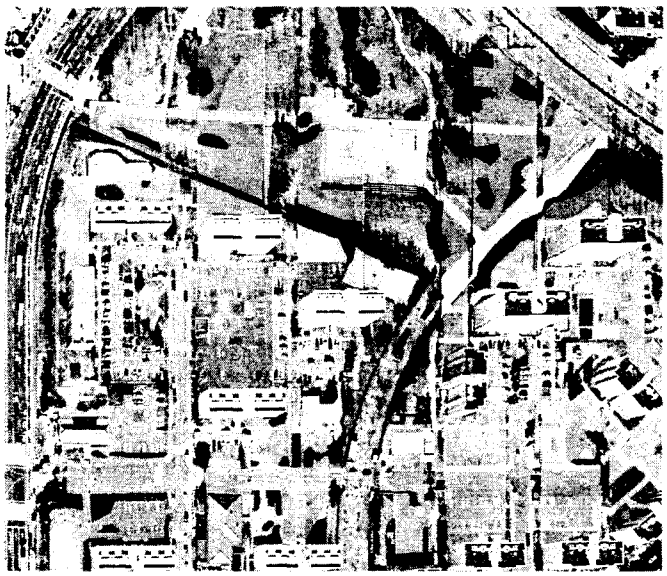

Fig. 10. shadow-free image

Table 2. Average & Standard Deviation of each feature

(Blue band)

Category	*Shadow*		*Non-Shadow*	
	Average	*Std.*	*Average*	*Std.*
Asphalt road	*118.55*	*20.27*	*196.50*	*19.65*
Unpaved road	*121.31*	*24.92*	*215.97*	*24.02*
Soil	*98.11*	*27.15*	*181.19*	*24.79*
Building	*172.86*	*29.11*	*242.30*	*11.81*
Trees	*72.34*	*19.60*	*122.00*	*22.42*

(Green band)

Category	*Shadow*		*Non-Shadow*	
	Average	*Std.*	*Average*	*Std.*
Asphalt road	*97.14*	*19.18*	*214.75*	*15.24*
Unpaved road	*95.53*	*15.15*	*244.88*	*9.39*
Soil	*80.05*	*19.26*	*223.16*	*17.03*
Building	*152.20*	*23.66*	*248.41*	*7.49*
Trees	*50.84*	*16.57*	*140.61*	*23.71*

(Red band)

Category	Shadow		Non-Shadow	
	Average	Std.	Average	Std.
Asphalt road	67.94	16.54	199.14	13.97
Unpaved road	67.00	15.70	238.70	11.69
Soil	66.13	20.25	236.44	11.78
Building	121.08	21.73	244.50	10.71
Trees	35.89	5.57	128.20	19.05

For the evaluation of correction of shadow effects, region growing method was used. As showed in Figure 1, the asphalt road has cast shadows. If the cast shadows of asphalt road were completely corrected, the road was detected as one feature including shadow regions in the case of being applied to region growing method. For the accurate test when region growing method is applied for images, the same seed pixel and threshold value are used. Figure 11 and figure 12 illustrate the result of this method for both. A dotted polygon was not including shadow regions in figure 11, however the asphalt road including non-shadowed region was detected as one polygon in figure 12.

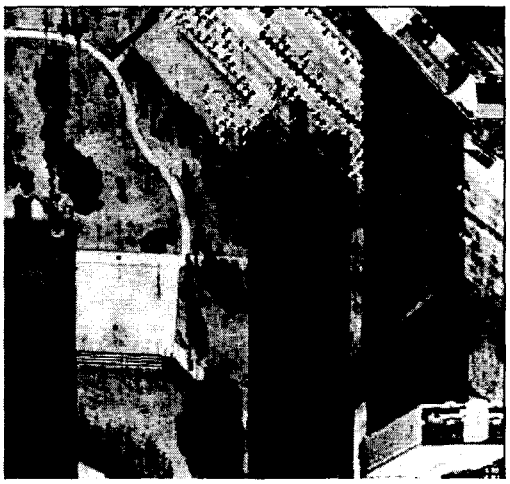

Fig. 11. results from region growing method for shadowed image

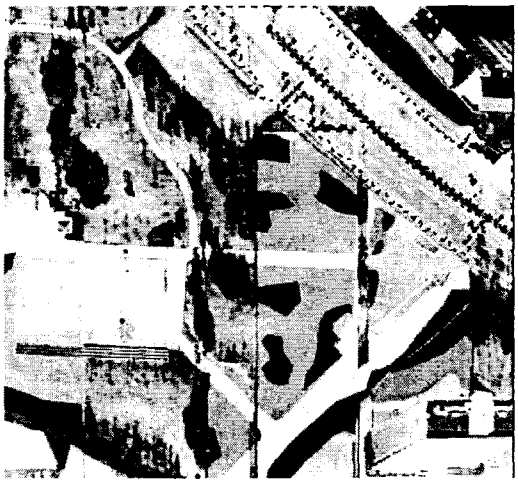

Fig 12. results from region growing method for non-shadowed image

Conclusion

In this study, the algorithms correcting shadows effects by combining digital map and LIDAR data. in aerial color image was described. It has been shown that the algorithms of shadow region delineation produced remarkable results in comparison with human interpretation. Also, shadow correction results can show us improved image interpretability. The proposed scheme achieves

- ·The correct delineation of cast shadows by using LIDAR data and shadow position with high accuracy
- ·The effectiveness of proposed shadow correction algorithms
- ·The enhancement of interpretability of aerial color image with shadow effects correction

References

Brown, D.C., 1991. Topoclimatic models of an apine environment using digital elevation models within a GIS, Proceedings, GIS/LIS '91 Conference, 28 Octorber-01 November, Atlanta, Geogia, 2:835-844.

Civco, D.L., 1991. Topographic normalization of Landsat Thematic Mapper digital imagery, Photogrammetric Engineering and Remote Sensing, 55(9):1303-1309.

Colby, J.D., 1991. Topographic normalization in rugged tarrain, Photogrammetric Engineering and Remote Sensing, 57(5):531-537.

Cowen, D.J., J. R. Jensen, C. Hendrix, M.E. Hodgson, and S.R. Schill. 2000. A GIS-Assisted rail Construction econometric model that incorporates LIDAR data. Photogrammetric Engineering and Remote Sensing, 66(11):1323-1328.

Crippen, R.E., R.G. blom, and P. Downey, 1981. Directed band ratioing for the retention of perceptually-independent topographic expression in chromaticity-enhanced imagery, International journal of Remote Sensing, 9(4):749-765

Giles, P.T., 2001 Remote Sensing and Cast Shadows in Mountainous Terrain, Photogrammetric Engineering and Remote Sensing, 67(7):833-839.

Stockham, J. T.G. ,1972, Image processing in the context of a visual model, Proceeding of the IEEE, 60, 828-842.

Polidorio, A.M, F. C. Flores, N. N. Imai, A .M. G. Tommaselli, and C. Fransco., 2003. automatic shadow segmentation in aerial color images, proceeding of the XVI Brazilian symposium on computer graphics and image processing,

Pouch, G.W. and D.J. Campagna, 1990. Hyperspherical direction cosine transformation for separation of spectral and illumination information in digital scanner data, Photogrammetric Engineering and Remote Sensing, 56(4):475-479.

Rau, J.Y., N.Y., chen, and L.C. Chen, 2002. True Orthophoto Generation of Built-Up Areas Using Multi-View Images. Photogrammetric Engineering and Remote Sensing, 68(6):581-588.

Richter, R., 1998. Correction of satellite imagery over mountainous terrain, Applied Optics, 37(18):4004-4015.